



# Preparation and properties of high temperature resistant neutron shielding poly(4-methyl-1-pentene)/boron carbide composite materials

Gu Huang<sup>1</sup> · Junjun Gong<sup>1</sup> · Wenming Xia<sup>1</sup> · Junjun Chen<sup>1</sup>

Received: 19 July 2022 / Accepted: 7 September 2022 / Published online: 11 October 2022  
© Akadémiai Kiadó, Budapest, Hungary 2022

## Abstract

To improve properties of the nuclear reactor secondary neutron shielding material, a novel high temperature resistant shielding material was prepared, in which poly(4-methyl-1-pentene) is blended with polyethylene and polypropylene as matrix materials and boron carbide as filler. Its neutron shielding properties were analyzed by Monte Carlo simulation and tested by Am–Be neutron source. Its thermodynamic properties were tested according to standard methods. Tests show that the new material's heat distortion temperature is up to 168 °C, which is much higher than that of polyethylene 45 °C and that of polypropylene 85 °C. The thermal neutron shielding performance of the new material is better than that of polyethylene.

**Keywords** Neutron shielding · High temperature resistance · Poly(4-methyl-1-pentene) · Monte Carlo

## Introduction

The reactor will generate a large amount of radiation during operation. In order to prevent neutrons and other rays with strong penetrating power from causing injury to professional workers, shielding protection is often used to reduce the risk of nuclear radiation exposure. Common neutron shielding materials include cement-based shielding materials, metal-based shielding materials, and polymer shielding materials [1]. High polymer shielding material is a composite material composed of hydrogen-rich polymer and some materials with excellent absorption of neutrons and secondary gamma rays. Polymer neutron shielding materials have the advantages of low density, simple processing technology and good shielding performance. When applied to ship reactors, small modular reactors and aerospace radiation shielding materials, lightweight materials can effectively improve mobility and reduce costs [2–8].

The thermodynamic properties and shielding properties of polymer composites are related to many factors. The main factors include the type of filler, the particle size of the

filler, the percentage of the composite material and dispersion [9–12]. Adeli Ruhollah et al. [13] studied the effect of boron carbide (B<sub>4</sub>C) particle size (20, 150 μm) on neutron shielding performance. Replacing 150 μm B<sub>4</sub>C filler with 20 μm B<sub>4</sub>C filler increases the thermal neutron shielding rate of the material by 5%. Zahra Soltani et al. [9] found that the penetrating rate of the composite material was reduced by about 40% when the nano-scale boron carbide particles were used to replace the micro-scale particles. Cataldo et al. [14] proposed to prepare a castable polyurethane (PUR) as a polymer matrix using polytetrahydrofuran polyol from renewable energy sources. The polymer was filled with 20.4% amorphous boron or 20.9% hexagonal boron nitride (h-BN) to prepare neutron shielding materials. The PUR composite prepared with amorphous boron shows the best shielding performances. The mass attenuation coefficient and linear attenuation coefficient of the amorphous boron PUR filled composite is 3.11 times and 2.24 times that of unfilled PUR.

Polyethylene-based composites are commonly used as secondary shielding materials for ship nuclear reactors. For example, lead-boron polyethylene materials are based on polyethylene (PE) doped with boron and lead. Its maximum withstand temperature is 80–100 °C. However, under some benchmark accident conditions, the temperature of reactor compartment may reach above 200 °C. At this time, the lead boron polyethylene material will have problems such as material deformation and softening.

✉ Wenming Xia  
xiawenming\_2008@163.com

<sup>1</sup> Naval University of Engineering, Liberation Avenue,  
Wuhan 430033, China

Poly(4-methyl-1-pentene) (TPX for short) is also a polyolefin material with a high proportion of hydrogen elements. Its Vicat softening temperature and melting temperature are 178 °C and 236 °C respectively. It shows that its thermal stability is higher than that of PE. Moreover, it can meet the heat resistance requirements of the secondary shielding material of the reactor [15–19].

In this study, TPX, PE, and polypropylene (PP) were used as the base materials, adding B<sub>4</sub>C as the filler. After necessary pre-processing of B<sub>4</sub>C, the composite materials were prepared by using a twin-screw extruder. The Monte Carlo software was used for simulation calculation. The prepared material was placed in the Am–Be neutron source field to test the neutron shielding performance [20, 21].

## Theory

The shielding of neutrons can be roughly divided into two processes: slowing down and capture or nuclear reaction. The former process is inelastic or elastic collision between neutrons and matter, in which neutrons' energy decrease. The latter process is that neutron is captured by matter or undergoes nuclear reaction.

To increase shielding performance, those materials with larger cross-section with neutrons are selected. For inelastic collision, elements with higher atomic number are preferred, such as lead, tungsten, etc. For elastic collision, hydrogen-rich materials are preferred, such as water, paraffin, high polymer, etc. For capture or nuclear reaction, though gadolinium (Gd), cadmium (Cd) and hafnium (Hf) have rather large neutron absorption cross-section, the energies of the secondary gamma rays are quite high. All three elements are rare and expensive, which limits their application as shielding material. Because boron is not expensive and the abundance of boron-10 is 19.8% whose cross-section of nuclear reaction with neutron is very large, and also the energy of secondary gamma ray produced during the nuclear reaction

is relatively low, boron is the best shielding material for absorbing neutron in most cases. Thus, boron carbide (B<sub>4</sub>C) is selected in this study [22].

## Monte Carlo simulation calculation

In order to obtain the optimized composition ratio, a model of mono-directional planar neutron source was established using MCNP4C, which is showed in Fig. 1. Shielding material, whose area is much larger than that of the detector and thickness is 4 cm is placed between source and detector. The energies vary from thermal neutron to 15 MeV and the detector uses F4 card for flux and F4 card combined with DE/DF card for dose. Figure 1 also shows neutrons emitted from source and after collision.

In order to explore the neutron shielding effect of shielding materials with different boron carbide contents, a variety of TPX-based shielding materials with different boron carbide contents were designed. The mass percentage of B<sub>4</sub>C ranges from 0 to 25%. The atomic ratios are shown in Table 1. Their performance indicators of shielding materials mainly include neutron dose shielding rate (DSR) and neutron penetrating rate (PR), whose definition is given by Eqs. (1) and (2).

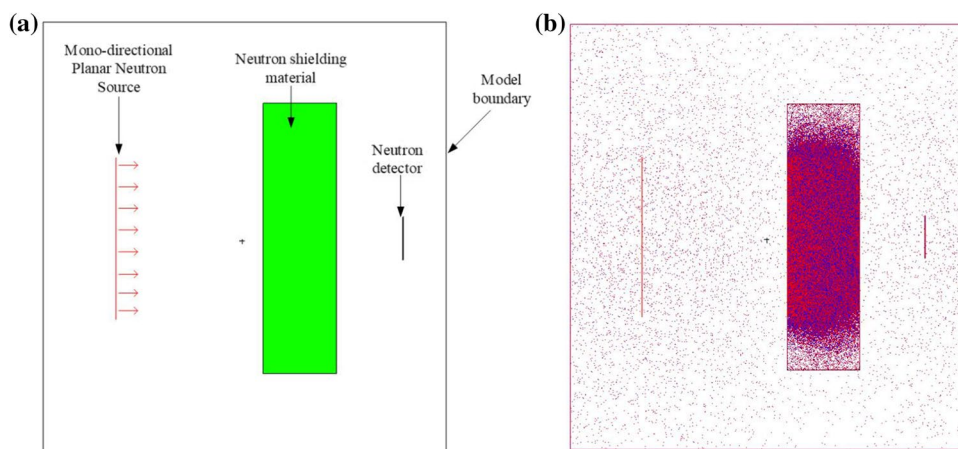
$$\text{DSR} = \left(1 - \frac{H}{H_0}\right) \times 100\% \quad (1)$$

$$\text{PR} = (I/I_0) \times 100\% \quad (2)$$

In Eq. (1),  $H$  is the dose equivalent rate measured with shielding material.  $H_0$  is the dose equivalent rate measured without shielding. In Eq. (2),  $I$  is the neutron flux measured with shielding material.  $I_0$  is the measured neutron flux without shielding.

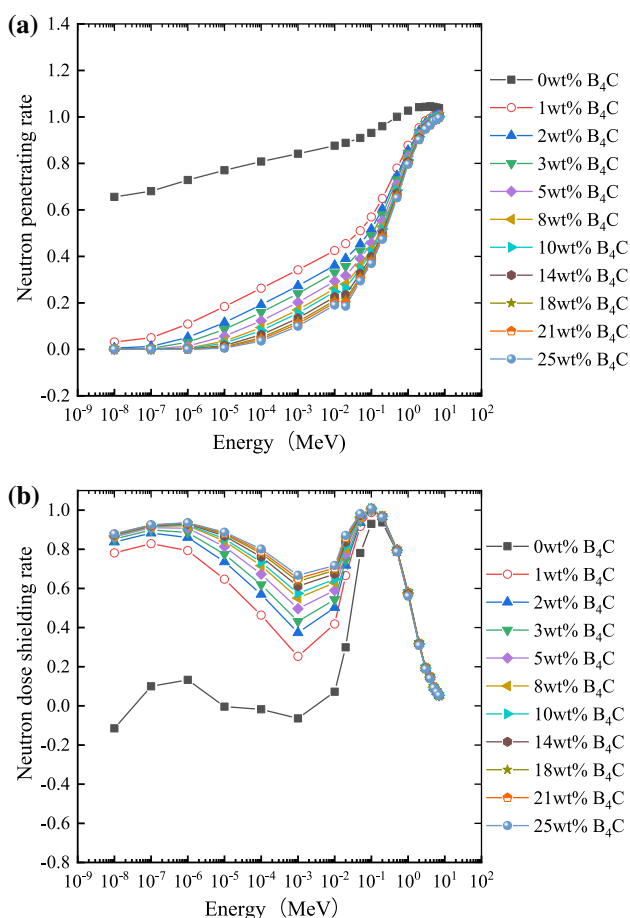
The calculation results are shown in Fig. 2. When the neutron energy is the same, the shielding performance of

**Fig. 1** MC model. **a** 2D model diagram, **b** Particle transport diagram



**Table 1** Atomic ratio of boron-containing TPX shielding materials

material code	Mass percentage of boron carbide %	$^{12}\text{C}$	$^1\text{H}$	$^{10}\text{B}$	$^{11}\text{B}$	Composite density(g/cm $^3$ )
1#	0	71.96	143.92	0	0	0.832
2#	1	71.42	142.48	0.15	0.58	0.838
3#	2	70.89	141.04	0.29	1.17	0.843
4#	3	70.35	139.61	0.44	1.75	0.849
5#	5	69.28	136.73	0.73	2.92	0.861
6#	8	67.67	132.41	1.16	4.68	0.879
7#	10	66.59	129.53	1.45	5.85	0.891
8#	14	64.44	123.77	2.03	8.19	0.918
9#	18	62.29	118.02	2.62	10.53	0.946
10#	21	60.68	113.70	3.05	12.28	0.968
11#	25	58.54	107.94	3.63	14.62	0.999

**Fig. 2** Calculation results of materials with different boron content. **a** neutron penetrating rate, **b** Neutron dose shielding rate

the material increases with the increase of B<sub>4</sub>C content. But the growth trend is gradually weakening with neutron energy increasing. The content of B<sub>4</sub>C has a great influence on low-energy neutrons. But the content of B<sub>4</sub>C has little effect on

high-energy neutrons. When the B<sub>4</sub>C content of the composite reaches 5 wt%, increasing the B<sub>4</sub>C content has limited effect on the shielding performance of the material. Taking into account performance and cost, the final choice of B<sub>4</sub>C content is 5 wt% in the material prepared in the subsequent experiments.

## Experimental

### Materials and equipment

Poly(4-methyl-1-pentene) was purchased from Mitsui, Japan. The density of TPX is only 0.83 g/cm<sup>3</sup>. The Vicat softening point of TPX is above 178 °C, and melting point is 230–240 °C. Linear polyethylene was purchased from Exxon Mobil Corporation whose density is 0.954 g/cm<sup>3</sup>. Polypropylene was purchased from Shandong Yousuo Chemical Technology Co., Ltd., China whose density is 0.92 g/cm<sup>3</sup>. B<sub>4</sub>C was purchased from Suzhou Yuante New Material Technology Co., Ltd., China. The particle size of B<sub>4</sub>C is 1 μm whose density is 3.48 g/cm<sup>3</sup>.

The B<sub>4</sub>C after surface modification were characterized by TENSOR II Fourier transform infrared spectrometer. The test wave number range is from 400 to 4000 cm<sup>-1</sup>. TGA/DSC analysis was performed on a Mettler-Toledo DSC-1 Star System using a conventional Al crucible with a punched lid under nitrogen flow at a heating rate of 5 °C/min.

The microstructure of the material was tested and characterized by scanning electron microscope. The samples were sprayed with gold for 45 s at 10 mA using Oxford Quorum SC7620 sputtering coater. A small number of samples were directly adhered to the conductive adhesive for observation. Then, ZEISS GeminiSEM 300 scanning electron microscope was used to photograph the morphology of the sample. The

acceleration voltage during shooting is 3 kV. The detector is SE2 secondary electronic detector.

### Preparation of composites

B<sub>4</sub>C is hydrophilic, while organic polymers such as TPX and PE are hydrophobic. During the blending process, particle agglomeration easily occurs due to the tension and van der Waals forces generated on the surface of the B<sub>4</sub>C particles. The wetting effect of B<sub>4</sub>C on TPX is poor. In order to improve the dispersibility of B<sub>4</sub>C, silane coupling agent KH-550 was used to modify the surface of B<sub>4</sub>C.

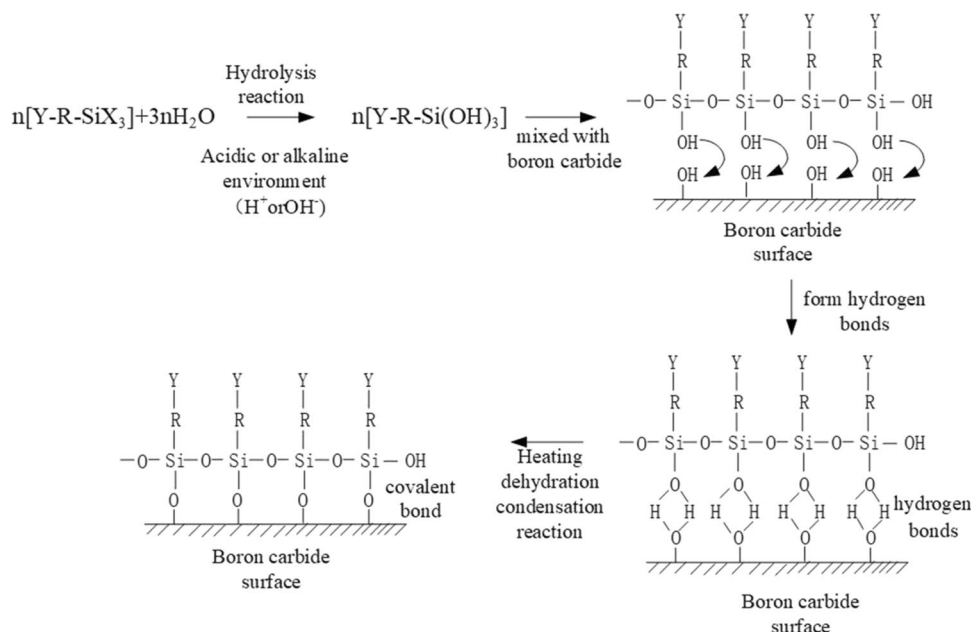
The operation steps of B<sub>4</sub>C surface modification experiment are as follows: (1) hydrolysis process: add absolute ethanol (24 mL), deionized water (8 mL) and 1 mL KH-550 reagent to the beaker. Stir to make it mixed evenly. Add additional acetic acid to adjust the pH to 6. Put the mixture into the ultrasonic cleaner. KH-550 reagent was completely hydrolyzed by ultrasonic vibration for 35 min. (2) Dehydration and condensation process: put the quantitative B<sub>4</sub>C into a boiling flask-3-neck. Then add absolute ethanol to soak B<sub>4</sub>C. Put the boiling flask-3-neck into the ultrasonic cleaning machine. Ultrasonic vibration for 35 min to fully mix. Pour the completely hydrolyzed solution in the beaker into a boiling flask-3-neck. Then place the boiling flask-3-neck in an oil bath at 80 °C. At the same time, use magnetic stirring for about 5 h. (3) Solid liquid separation and dry: vacuum filter is used for multiple suction filtration to clarify the solution. Solid and liquid are completely separated. Finally, the obtained modified B<sub>4</sub>C solid was directly put into the oven and dried at 100 °C for about 8 h. The possible chemical reactions in the modification process are shown in Fig. 3.

Melt blending method was used in this study. Use a mixer to mix TPX, PE, PP and modified B<sub>4</sub>C according to the proportion in Table 2. The price of TPX is several times more expensive than PE and PP. Adding PE and PP can reduce the cost and improve the density of the composite material, while heat resistance is deterioration. When setting the ratio of TPX to PE or PP, the content of TPX in the composite material should be reduced as much as possible under the premise of meeting the heat resistance requirements. The mass percentage of TPX in the composite was set between 31 and 72%. The mixture is then added to a twin-screw extruder for kneading. Pour the material mixed by the extruder into the steel mold. After closing the mold manually, put the mold into the vulcanizer for heating and pressing to obtain the final sample. The maximum extrusion temperature of the extruder is 275 °C. The extrusion pressure was 25 MPa. The size of the flat-shaped mold is 15 × 15 × 1 cm. The size of the dumbbell mold is the sample

**Table 2** Composition table of composite materials per 100 g

Material code	TPX (g)	PE (g)	PP (g)	B <sub>4</sub> C (g)
1	31.67	63.33	0	5
2	47.5	47.5	0	5
3	63.33	31.67	0	5
4	71.25	23.75	0	5
5	31.67	0	63.33	5
6	47.5	0	47.5	5
7	63.33	0	31.67	5
8	71.25	0	23.75	5

**Fig. 3** Modification reaction process



size in the standard of ASTM D638 Tensile Properties of Plastics.

### Experiments on neutron shielding effect

Using the laboratory Am–Be neutron source as the radioactive source, an experimental platform was built for neutron shielding experiments. The Am–Be neutron source is from HTA Co., Ltd. The neutron source activity is  $1.85 \times 10^{10}$  Bq, and the neutron emission rate is  $1 \times 10^6$  per second. The experimental platform consists of neutron source, shielding material and neutron detector. The experimental site photo is shown in Fig. 4. The dose equivalent and neutron flux were measured with a neutron dosimeter and a long neutron counter, respectively. The long neutron counter based on  $\text{BF}_3$  proportional counter is used. The long neutron counter cooperates with the data acquisition and display software LC1101N to obtain the neutron flux. The long neutron counter and software are from Nuclover Technology (Beijing) Co., Ltd. The neutron dose meter is an NDM-A portable neutron dose equivalent meter. The detector uses a helium-3 proportional metal counter tube as the detection element, the neutron moderator is made of polyethylene material, the neutron absorber is made of boron-containing plastic, and the casing is made of nickel-plated aluminum alloy. The neutron dose meter is from Beijing Nuc-safe Technology Co., Ltd. When the neutron energy is in the energy range of 0.22–5 MeV, the detection efficiency deviation of the long neutron counter is within  $\pm 10\%$ . The dose equivalent rate measured under neutron shadow cone conditions is the dose equivalent rate produced by scattered neutrons. This dose equivalent rate should be subtracted from the final measurement. The neutron dose shielding rate and neutron penetrating rate of the material were calculated by Eqs. (1) and (2).

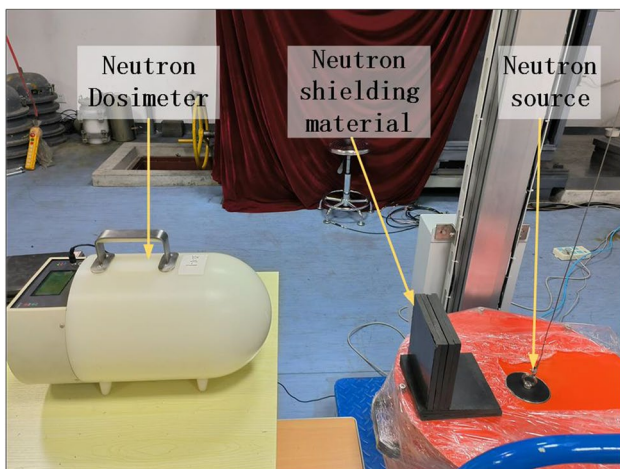


Fig. 4 Site map of neutron shielding experiment

## Results and discussion

### Characterization of $\text{B}_4\text{C}$ modification results by FT-IR

In order to verify the effect of particle surface modification and observe the adhesion of filler functional group particles, the particles were measured by Fourier transform infrared spectroscopy. The test results are shown in Fig. 5.

As shown in Fig. 5, the upper curve is the FT-IR spectrum of the modified  $\text{B}_4\text{C}$  raw material. The intermediate curve is the FT-IR spectrum of unmodified  $\text{B}_4\text{C}$  raw material. The lower curve is the FT-IR spectrum of silane coupling agent KH-550 (using the original layer to compare the three groups of data). Compared with the unmodified  $\text{B}_4\text{C}$  raw material, the curve after surface modification has two weak absorption peaks at  $2929 \text{ cm}^{-1}$  and  $2885 \text{ cm}^{-1}$ , which should be due to the antisymmetric stretching vibration absorption bands of methylene and methyl. The characteristic peak at  $1087 \text{ cm}^{-1}$  is enhanced, which is the result of the overlap of B–C and Si–O bonds in boron carbide. In addition, the wide peak at  $1555 \text{ cm}^{-1}$  is the result of N–H overlap. The results of single peak show that the surface properties of the treated boron carbide filler have changed. Each enhancement peak corresponds to the functional group in KH-550, which indicates that the surface modification of boron carbide by KH-550 is achieved. The alkoxy group on the coupling agent forms a covalent bond with  $\text{B}_4\text{C}$ . Silane molecules bind to the surface of  $\text{B}_4\text{C}$  and polymerize. In the process of material mixing and preparation, the presence of silane molecules will make  $\text{B}_4\text{C}$  more closely bound to organic materials.

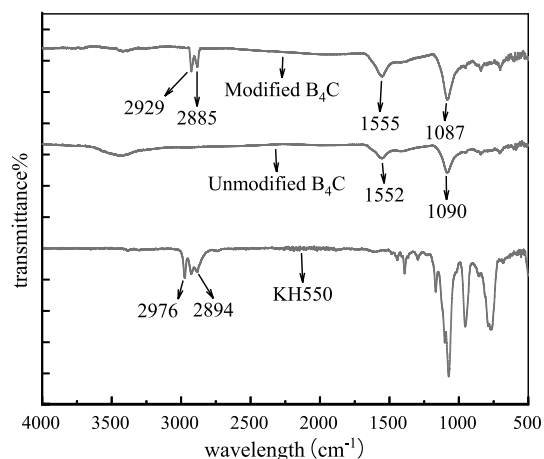


Fig. 5 FT-IR spectra of  $\text{B}_4\text{C}$  raw material and modified  $\text{B}_4\text{C}$

## Basic physical properties and microscopic morphology of composites

The secondary shielding material of the reactor is usually used for the cladding of the containment (the bulkhead of the reactor compartment). The mechanical strength and thermodynamic properties of materials shall meet the index requirements of non-load bearing building materials. In addition, in order to ensure the safety of workers around the reactor, it is required that in the event of a small LOCA accident, the secondary shielding material of the reactor can still effectively shield neutrons without deformation under high temperature conditions. Therefore, the thermodynamic properties of the composites were tested, including tensile properties and hardness. The experimental test results of material performance parameters are shown in Table 3.

The hardness and tensile strength of the material increased with increasing TPX content. This is inseparable from the excellent performance of TPX itself. The hardness value of the composite material can reach above 66, which can meet the requirements of the secondary shielding material. The measured value of the material density is lower than the theoretical value, which may be due to the existence of small air bubbles inside the composite. However, the porosity of the materials is below 3.7%. The minimum is only 1.71%, which indicates that the combination of filler and substrate is good. Material No. 6 has the lowest porosity, high hardness, highest tensile strength and best performance. This shows that the binding performance of TPX and PP is better than that of PE. And the optimal ratio is 2:1.

The morphology of the samples was photographed with a ZEISS GeminiSEM 300 scanning electron microscope. The microscopic morphologies of TPX/PE/B<sub>4</sub>C composites and TPX/PP/B<sub>4</sub>C composites were obtained, as shown in Fig. 6. The spherical particles in Fig. 6a, b are B<sub>4</sub>C particles with a maximum particle size of 2 μm, indicating that the agglomeration phenomenon is not obvious. This also reflects that the surface modification effect is good, making the filler distribution uniform. There are few small holes in the figure, and the radius of the small holes in the upper right is less

than 0.5 μm, indicating that the material has low porosity and good preparation process. The microscopic morphology of the TPX/PP/B<sub>4</sub>C composite in Fig. 6c, d is layered, indicating that the binding strength and compatibility of TPX combined with PP are better than PE. The surface of the material is very smooth, indicating that the filler is evenly distributed.

## Thermal performance analysis

In order to explore the temperature resistance of composite materials with different ratios, TG/DSC analysis was carried out on the materials in this study. From the TG/DSC curve, the melting and mass loss of the composite can be seen very intuitively. The compatibility of TPX and PE can be analyzed. The TG curve of the sample is shown in Fig. 7, and the DSC curve is shown in Figs. 8 and 9.

It can be seen from the analysis in Fig. 7 that during the heating process of the material from room temperature to 650 °C, the TGA loss rate is all within 93.48%–95.3%. The thermal decomposition temperature of TPX, PE and PP is low, and the residual rate should be 0% when the temperature reaches 650 °C. The melting point of B<sub>4</sub>C is as high as 2350 °C. The mass loss of B<sub>4</sub>C will not change significantly at 650 °C. Therefore, the content of residual B<sub>4</sub>C should be 5%. The reason why the residual part of the sample is less than 5% may be that the organic part takes away some B<sub>4</sub>C in the aluminum crucible during the volatilization process. The sample is 10 mg of material randomly selected from 200 g of sample material, which reflects that B<sub>4</sub>C is evenly dispersed in the material. During the heating process from room temperature to 350 °C, the mass loss of the sample is less than 0.5%. It shows that the thermal stability of the composite material is good. The thermal decomposition temperatures (5% thermogravimetric loss temperature) of samples 1–8 were 410.7 °C, 410.9 °C, 405.5 °C, 408.7 °C, 411.2 °C, 413.2 °C, 416.1 °C, 412.5 °C. With the increase of TPX content, the thermal decomposition temperature of the materials first increased and then decreased. Sample 7 has the best heat resistance, indicating that when the ratio

**Table 3** Tensile properties of composites

Material code	Hardness	Tensile strength (Mpa)	Elongation at break (%)	Actual density (g/cm <sup>3</sup> )	Theoretical density (g/cm <sup>3</sup> )	Porosity
1	66.7	13.51	1.2	0.928	0.944	1.71%
2	67.5	14.34	1.3	0.898	0.923	2.72%
3	69.4	18.52	2.2	0.880	0.903	2.50%
4	71.4	21.03	1.5	0.861	0.893	3.63%
5	76.0	20.59	1.5	0.892	0.910	2.00%
6	77.5	27.40	2.5	0.886	0.898	1.38%
7	77.3	20.45	2.3	0.857	0.887	3.38%
8	76.6	18.32	1.9	0.854	0.881	3.10%

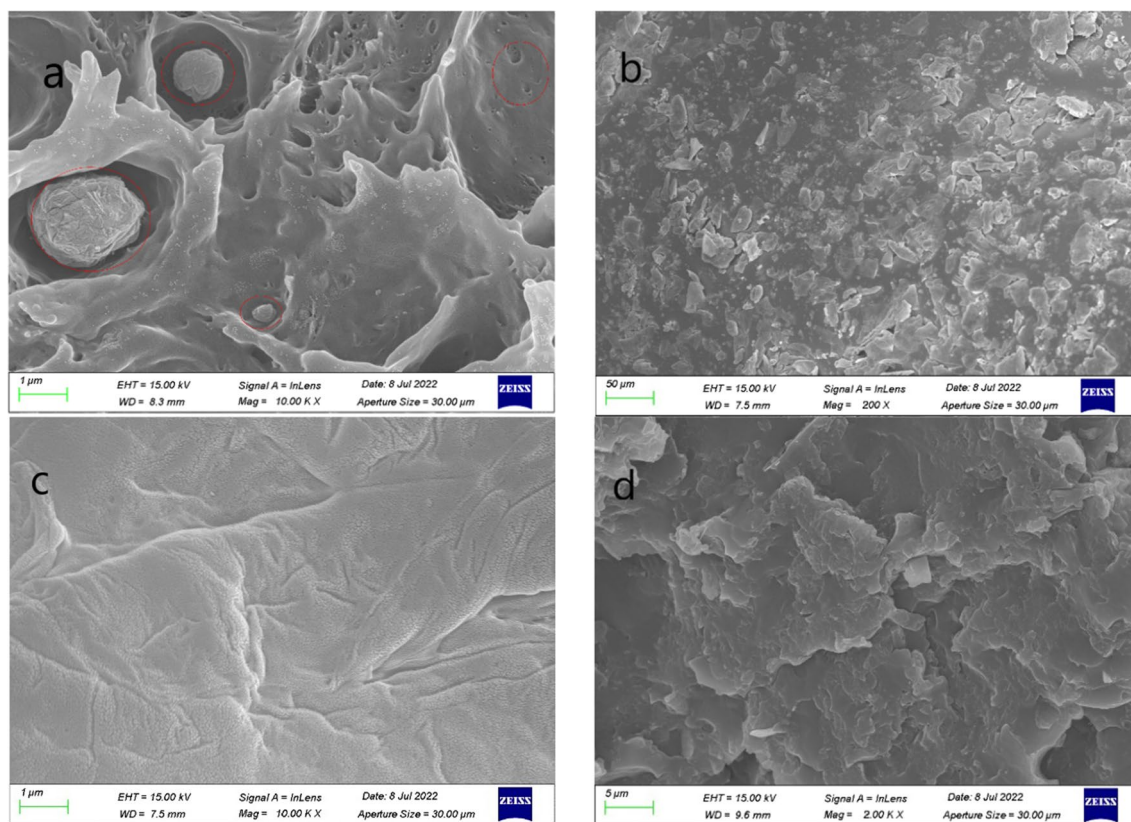


**Fig. 6** a, b Micromorphology of TPX/PE/B<sub>4</sub>C composites. c, d Micromorphology of TPX/PP/B<sub>4</sub>C composites

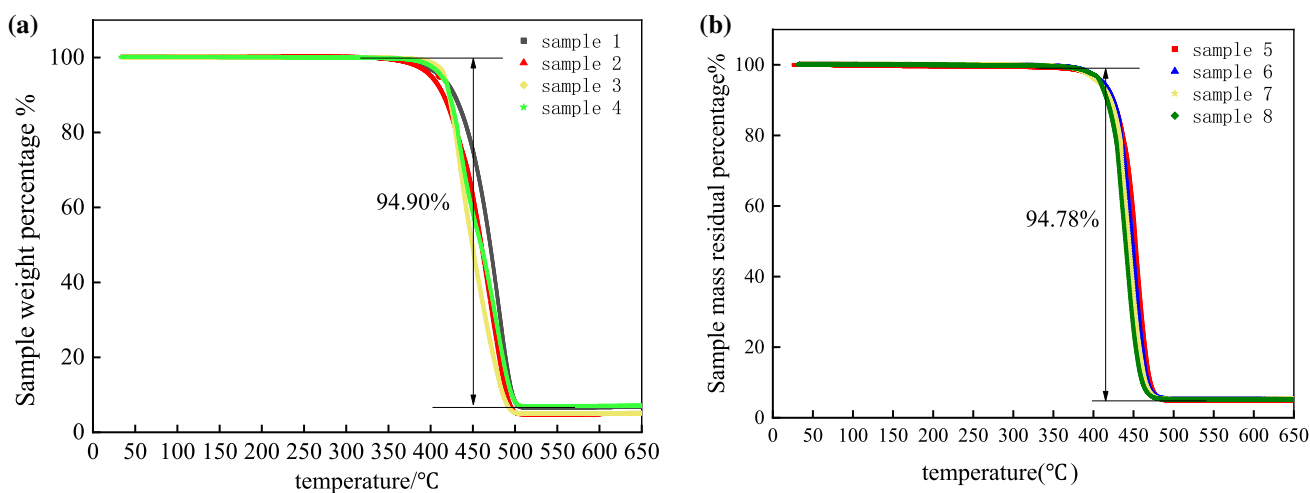


**Fig. 7** TG curve of the sample. a TG curve of the TPX/PE blend composites, b TG curve of the TPX/PP blend composites

of TPX and PP is 2:1, the molecular structure is stabler and the blending effect is better.

There are two peaks in the DSC heating curves of materials with different ratios in Figs. 8 and 9. From left to right are the melting peaks of PE (or PP) and TPX, respectively.

The peak broadening and peak position did not change much with the increase of TPX content. According to the data provided by the manufacturer, the melting point of pure PE is 110 °C, and the melting point of pure PP is 150 °C. The melting temperature of PE in the composite material

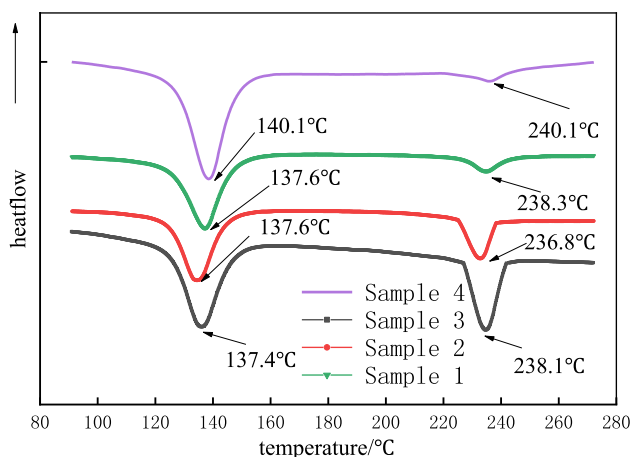


**Fig. 8** DSC curve of the TPX/PE blend composites

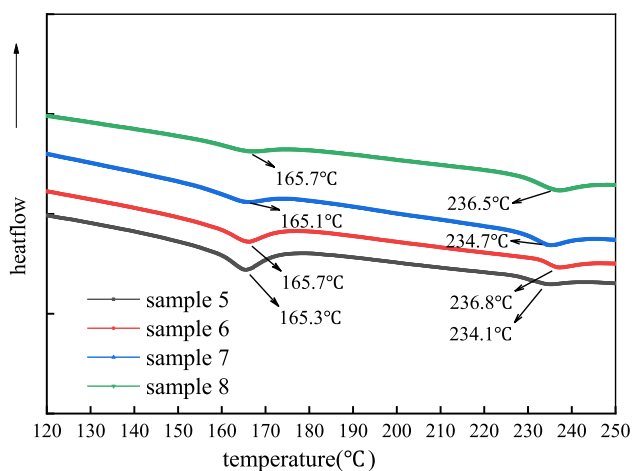


**Fig. 9** DSC curve of the TPX/PP blend composites

ranges from 125 to 145 °C, and the melting temperature of PP ranges from 160 to 170 °C. Compared with the pure components, the melting temperature of the blended PP or PE is increased by 10–20 °C. The melting temperature of TPX ranges from 230 to 240 °C. Therefore, TPX has a heterogeneous nucleation effect on PE or PP, which indicates that TPX is compatible with PE or PP. According to the principle of equilibrium melting point, the melting temperature range of the composite material should be between TPX and PP or PE, and it is related to the ratio of materials.

The heat distortion temperature of the materials was tested by standard ASTM D648, ISO75. The test pressure is 1.8 MPa, the sample size is 80 mm × 10 mm × 4 mm, and

the heating rate is 2 °C/min. The heat distortion temperature of the eight materials is shown in Table 4.

The heat distortion temperature of PE is 40–50 °C, and that of polypropylene is 85–104 °C. The heat distortion temperature of TPX/PP/B<sub>4</sub>C composites and TPX/PE/B<sub>4</sub>C composites is much higher than that of PE. However, the heat distortion temperature of TPX is 170–180 °C. The heat distortion temperature of the composites is slightly lower than that of TPX and increases with the increase of TPX content.

## Neutron shielding performance

The neutron shielding properties of the composites were characterized by a monoenergetic source shielding simulation experiment and an Am–Be source fast neutron shielding experiment. The simulation calculation results of monoenergetic neutron shielding are shown in Fig. 10. The second point from left to right in the figure is the calculation result of thermal neutron source (neutron energy  $2.5 \times 10^{-8}$  MeV). The data shows that the shielding effect of different proportions of materials has a small gap. The 4 cm-thick shielding material has a dose shielding rate of more than 98% for thermal neutrons, which is 8% higher than that of pure PE. This shows that the thermal neutron shielding performance of the composite material is good.

In the fast neutron shielding experiment of Am–Be source, the results of the neutron dose shielding rate of the material are shown in Fig. 11a, b. The neutron penetrating rate results of the material are shown in Fig. 11c. As the material thickness increases, the neutron dose shielding efficiency continues to improve. The neutron shielding properties of the eight shielding materials are not very different, and they are all comparable to PE. As shown in Fig. 11a, With the increase of TPX content in TPX/PE/B<sub>4</sub>C composites, the shielding effect decreased slightly. The fast neutron shielding rate of 4 cm thick material is close to 50%, indicating that the fast neutron shielding effect of the material is good. As shown in Fig. 11b, with the increase of TPX content in TPX/PP/B<sub>4</sub>C composites, the fast neutron shielding performance changes little. The neutron dose shielding rate of the new composite is 3–5% lower than that of PE.

The average energy of the Am–Be neutron source is 4.2–5 MeV. It can be seen from Fig. 10 that when the neutron source energy is 4.2–5 MeV, the neutron dose shielding rate calculated by the simulation of the material is between 40 and 50%. The relative deviation between the simulation calculation results and the actual Am–Be neutron source experiment results is within 10%. Since the measurement

**Table 4** The heat distortion temperature composite materials

Material code	1	2	3	4	5	6	7	8
Heat distortion temperature (°C)	136.7	144	145.55	156.75	147.8	155.65	158.8	168



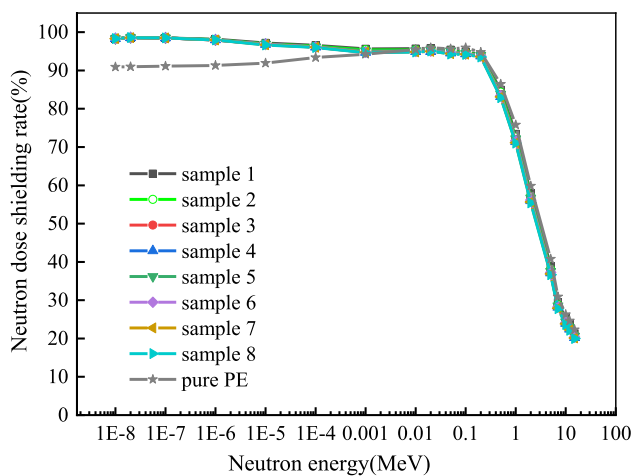


**Fig. 10** Simulation results of monoenergetic neutron shielding

error of the neutron dosimeter is  $\pm 10\%$ , it can be considered that the results of the simulation experiment and the actual experiment are consistent.

The shielding effect of fast neutrons is related to the material density and the hydrogen content of the material, while the density of the eight materials varies little. Therefore, the shielding effect of each material is not very different. The neutron penetrating rate of 4 cm thick material is between 50 and 55%.

### Conclusion

In this study, the optimal ratio of TPX-based composites was obtained through Monte Carlo software simulation calculation. Considering neutron shielding performance and economy, the mass percentage of boron carbide is preferably 5%. The novel materials are prepared using a screw

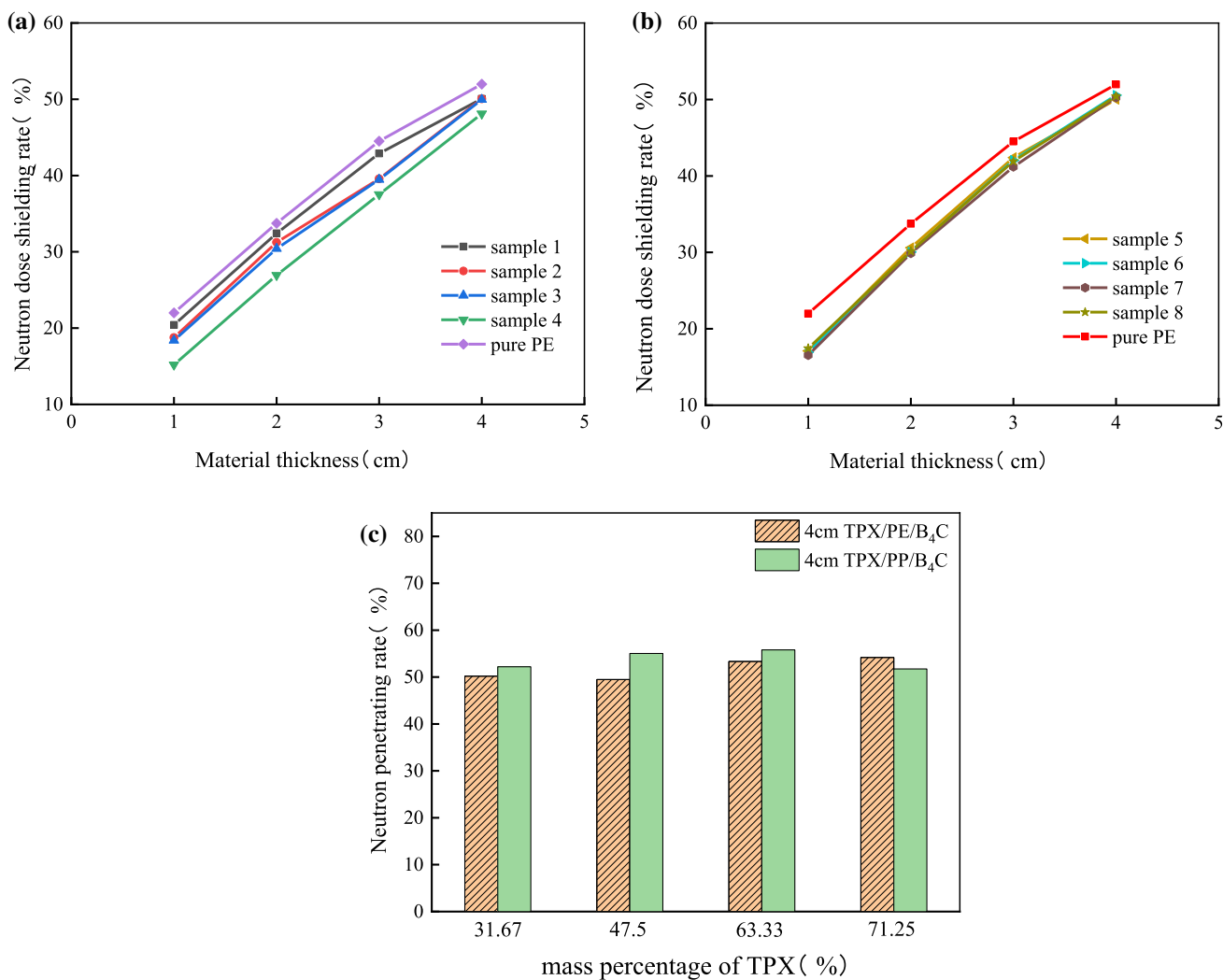


**Fig. 11** Shielding performance for Am–Be neutron source. **a, b** Neutron dose shielding rate of material. **c** neutron penetrating rate of material

extrusion process by blending PP/PE with TPX and doping B<sub>4</sub>C. The porosity of the composites is all below 3.6%. The microstructure and mechanical properties of the composites show that the fillers are uniformly distributed in the composites and tightly combined. The heat distortion temperature of the new composites is up to 168 °C. The results show that the thermal properties of the composite material have great advantages compared with PE, and the heat resistance of TPX/PP/B<sub>4</sub>C composites is better than that of TPX/PE/B<sub>4</sub>C composites. The thermal neutron dose shielding rate of the 4 cm-thick composite material exceeds 98%. However, the thermal neutron dose shielding rate of PE with a thickness of 4 cm is less than 90%. The simulation data show that the thermal neutron shielding properties of TPX/PP/B<sub>4</sub>C composite and TPX/PE/B<sub>4</sub>C composite are better than those of PE. The fast neutron penetrating rate of the 4 cm-thick composite material is lower than 55%, and the fast neutron dose shielding rate is up to 50%. The fast neutron shielding rate of the new composites is 3–5% lower than that of PE, which is mainly due to the slightly higher density of PE. Thermal and fast neutrons can be effectively shielded by TPX-based composites. Especially the thermal neutron shielding performance is more prominent. The excellent thermodynamic properties and thermal neutron shielding properties of the new material make it a competitive potential choice for ship reactor secondary shielding.

## Declarations

**Conflict of interest** The authors have no relevant financial or non-financial interests to disclose.

## References

- Abdulrahman ST, Ahmad Z, Thomas S et al (2020) Chapter 1—Introduction to neutron-shielding materials. In: Abdulrahman, Thottathil S, Thomas S, Ahmad Z (eds) Micro and nanostructured composite materials for neutron shielding applications. Woodhead Publishing, Sawston, pp 1–23
- Wang Z, Liu C, Fang G et al (2021) Vitrification of nuclear contaminated lead–boron polyethylene. *J Non Cryst Solids*. <https://doi.org/10.1016/j.jnoncrsol.2021.120832>
- Umm-E-Kulsoom GSA, Khurshid MS et al (2020) Investigating the effect of adding CdO nano particles on neutron shielding efficacy of HDPE. *Radiat Phys Chem* 177:109–145
- Uddin Z, Yasin T, Shafiq M et al (2020) On the physical, chemical, and neutron shielding properties of polyethylene/boron carbide composites. *Radiat Phys Chem* 166:108–450
- Tuna T, Eker AA, Kam E (2021) Neutron shielding characteristics of polymer composites with boron carbide. *J Korean Phys Soc*. <https://doi.org/10.1007/s40042-021-00089-z>
- Guru S, Amritphale SS, Mishra J, Joshi S et al (2019) Multi-component red mud-polyester composites for neutron shielding application. *Mater Chem Phys*. <https://doi.org/10.1016/j.matchemphys.2018.12.039>
- Özdemir T, Akbay SK, Uzun H et al (2016) Neutron shielding of EPDM rubber with boric acid: mechanical, thermal properties and neutron absorption tests. *Prog Nucl Energy* 89:102–109
- Mülazim Y, Kızılkaya C, Kahraman MV (2011) Thermal and neutron shielding properties of 10B2O3/polyimide hybrid materials. *Polym Bull*. <https://doi.org/10.1007/s00289-011-0481-4>
- Soltani Z, Beigzadeh AM, Ziaie F et al (2016) Effect of particle size and percentages of boron carbide on the thermal neutron radiation shielding properties of HDPE/B<sub>4</sub>C composite: experimental and simulation studies. *Radiat Phys Chem* 127:182–187
- Shin JW, Lee J-W, Yu S et al (2014) Polyethylene/boron-containing composites for radiation shielding. *Thermochim Acta*. <https://doi.org/10.1016/j.tca.2014.03.039>
- Baxter L, Herrman K, Panthi R et al (2020) Chapter 3—Thermoplastic micro and nanocomposites for neutron shielding. In: Abdulrahman ST, Thomas S, Ahmad Z (eds) Micro and nanostructured composite materials for neutron shielding applications. Woodhead Publishing, Sawston, pp 53–82
- Korkut T, Karabulut A, Budak G et al (2010) Investigation of fast neutron shielding characteristics depending on boron percentages of MgB<sub>2</sub>, NaBH<sub>4</sub> and KBH<sub>4</sub>. *J Radioanal Nucl Chem*. <https://doi.org/10.1007/s10967-010-0619-0>
- Adeli R, Shirmardi SP, Ahmadi SJ (2016) Neutron irradiation tests on B<sub>4</sub>C/epoxy composite for neutron shielding application and the parameters assay. *Radiat Phys Chem* 127:140–146
- Cataldo F, Prata M (2019) New composites for neutron radiation shielding. *J Radioanal Nucl Chem*. <https://doi.org/10.1007/s10967-019-06526-5>
- Griffith JH, Rånby BG (1960) Dilatometric measurements on poly(4-methyl-1-pentene) glass and melt transition temperatures, crystallization rates, and unusual density behavior. *J Polym Sci*. <https://doi.org/10.1002/pol.1960.1204414408>
- Tanigami T, Yamaura K, Matsuzawa S et al (1986) Thermal expansion of crystal lattice of isotactic poly(4-methyl-1-pentene). *Polym J* 18:35–40
- Jebaseelan Samuel EJ, Mohan S (2004) FTIR and FT Raman spectra and analysis of poly(4-methyl-1-pentene). *Spectrochim Acta A* 60:19–24
- Bu H, Qiu W, Tan Z et al (2015) Study on toughening of poly(4-methyl-1-pentene) with various thermoplastic elastomers. *J Thermoplast Compos Mater* 28:1334–1342
- Xu LY, Ma AP, Yin B et al (2019) The effect of alkylated graphene oxide on the crystal structure of poly(4-methyl-1-pentene) during uniaxial deformation at high temperature. *Polym Compos* 40:E493–E500
- Guembou Shouop CJ, Ndongchueg Moyo M, Nguelem Mekongtso EJ et al (2021) 241Am/Be source optimum geometry for DSRS management-based Monte Carlo simulations. *AIP Adv* 11:115–124
- Karimi-Shahri K, Rafat-Motavalli L, Miri-Hakimabad H (2013) Finding a suitable shield for mixed neutron and photon fields based on an Am–Be source. *J Radioanal Nucl Chem*. <https://doi.org/10.1007/s10967-012-2225-9>
- Kipcak AS, Gurses P, Derun EM et al (2013) Characterization of boron carbide particles and its shielding behavior against neutron radiation. *Energy Convers Manag*. <https://doi.org/10.1016/j.enconman.2012.08.026>

**Publisher's Note** Springer Nature remains neutral with regard to jurisdictional claims in published maps and institutional affiliations.

Springer Nature or its licensor holds exclusive rights to this article under a publishing agreement with the author(s) or other rightsholder(s); author self-archiving of the accepted manuscript version of this article is solely governed by the terms of such publishing agreement and applicable law.